Chemical Science

ROYAL SOCIETY OF CHEMISTRY

EDGE ARTICLE

View Article Online
View Journal | View Issue





Cite this: *Chem. Sci.*, 2024, **15**, 5980

All publication charges for this article have been paid for by the Royal Society of Chemistry

Received 10th October 2023
Accepted 6th March 2024

DOI: 10.1039/d3sc05357a

rsc.li/chemical-science

# Electrosynthesis of iminophosphoranes and applications in nickel catalysis†

Velabo Mdluli, [a] Dan Lehnherr, *[a] Yu-hong Lam, *[b] Mohammad T. Chaudhry, [c] Justin A. Newman, [c] Jimmy O. DaSilva [c] and Erik L. Regalado [c]

P(v) iminophosphorane compounds are accessed *via* electrochemical oxidation of commercially available P(III) phosphines, including mono-, di- and tri-dentate phosphines, as well as chiral phosphines. The reaction uses inexpensive bis(trimethylsilyl)carbodiimide as an efficient and safe aminating reagent. DFT calculations, cyclic voltammetry, and NMR studies provide insight into the reaction mechanism. The proposed mechanism reveals a special case of sequential paired electrolysis. DFT calculations of the frontier orbitals of an iminophosphorane are compared with those of the analogous phosphines and phosphine oxides. X-ray crystallographic studies of the ligands as well as a Ni-coordination complex provide structural insight for these ligands. The utility of these iminophosphoranes as ligands is demonstrated in nickel-catalyzed cross-electrophile couplings including C($sp^2$)–C($sp^3$) and C($sp^2$)–C($sp^2$) couplings, an electrochemically driven C–N cross-coupling, and a photochemical arylative C($sp^3$)–H functionalization. In some cases, these new ligands provide improved performance over commonly used $sp^2$-*N*-based ligands (*e.g.* 4,4′-di-*tert*-butyl-2,2′-bipyridine).

## Introduction

Phosphorus-containing compounds are ubiquitous in catalysis,[1] particularly as phosphorus(III)-based ligands in transition metal catalysis.[2,3] However phosphorus(v) compounds are relatively underexplored as ligands or catalysts. Phosphine oxide (P=O) ligands have been featured in Pd-couplings[4–7] and asymmetric Cu-catalysed alkylation[8] of imines and nitroalkenes (see ESI Fig. S1† for additional details). P(v)-containing structures have also been used as organocatalysts, including the use of phosphine oxide-based catalysts for enantioselective aldol reactions.[9] P=S and P=Se based phosphorimide catalysts have been used to mediate per-silylation of 2′-deoxynucleosides to access the corresponding glycals.[10] P=N based structures such as iminophosphoranes are known but represent an underutilized class of ligands in earth-abundant metal catalysis.[11] There are exciting results of utilizing iminophosphoranes as ligands in catalytic cross-coupling reactions (*e.g.*, Sonogashira,[12] Suzuki-Miyaura,[13] Kumada,[14] and Negishi couplings[14b]) and hydrogenations of alkene,[15] and ketones,[16] cyclopropanation,[17] alkene oligo- and polymerizations,[18] ring opening polymerizations (*e.g.* lactide, ε-caprolactone),[19] as well as in organocatalysis,[20] amongst others.[11] Scheme 1 illustrates a selection of these examples. Iminophosphoranes have also been used as organic neutral super-electron donors in organic synthesis.[21]

Despite their appeal in catalysis, access to iminophosphoranes remains limited, in stark contrast to the hundreds of commercially available P(III) ligands. The relative scarcity of applications of iminophosphoranes can be attributed to difficulty in their synthesis (*e.g.* hazardous reagents), limited access to commercially available precursors, and limited reaction scope. Scheme 1E illustrates a variety of commonly used synthetic approaches to iminophosphoranes. For example, synthesis through Staudinger reaction[22] involves the use of azides which are potentially explosive, and requires one or more steps to access the requisite azide. Other approaches to iminophosphoranes include the Kirsanov reaction[23] starting from hazardous $PCl_5$, and the modified Kirsanov reaction,[11,24] which relies on a two-step bromination–amination process of a phosphine. Other approaches exist with limited scope, such aminations facilitated by diethylazodicarboxylate,[25] which is also a hazardous and shock-sensitive reagent.[26] More recent approaches to iminophosphoranes have included the photolytic generation of nitrenes from bespoke dibenzothiophene *N*-substituted sulfilimine or dioxazolones reagents.[27] More recently, the use of *N*-pivaloyloxybenzamide and iron catalysis

[a]*Process Research and Development, Merck & Co., Inc., Rahway, New Jersey 07065, USA. E-mail: dan.lehnherr@merck.com*

[b]*Modeling and Informatics, Merck & Co., Inc., Rahway, New Jersey 07065, USA. E-mail: yu.hong.lam@merck.com*

[c]*Analytical Research and Development, Merck & Co., Inc., Rahway, New Jersey 07065, USA*

† Electronic supplementary information (ESI) available. CCDC 2259466, 2259467, 2258974, 2258975, 2258976, 2258977, 2258978, 2258979, 2258980 and 2329725. For ESI and crystallographic data in CIF or other electronic format see DOI: https://doi.org/10.1039/d3sc05357a

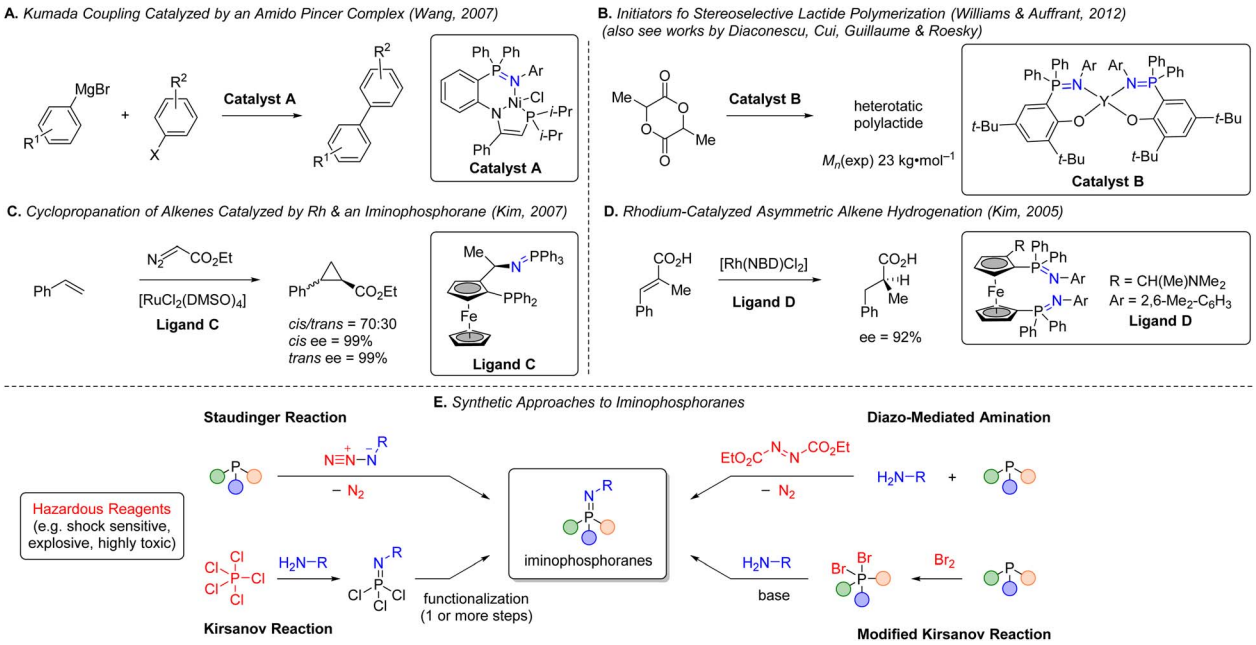


Scheme 1 (A–D) Applications of iminophosphoranes as ligands in catalysis. (E) Synthetic approaches to iminophosphoranes.

was reported access *N*-acyl iminophosphoranes.[28] Morandi reported a related approach using hydroxylamine-derived triflic acid salt to access iminophosphorane triflic acid salts.[29] Ultimately, safe and scalable methods with broad scope are in high demand. To address these limitations, we wondered whether electrochemistry[30] could be used to convert commercially available P(III) ligands to P(V) iminophosphorane sp$^2$-*N*-ligands (Scheme 2A) *via* an environmentally sustainable and operationally simple and safe process. The potential to access novel iminophosphorane-containing P=N ligands from readily available phosphines would quickly expand the diversity of bi- and tridentate ligands in analogy to the classic sp$^2$-nitrogen-based bipyridine and terpyridine ligands (Scheme 2B), which are gaining popularity in base-metal catalysis. Herein, we report an electrochemical method to access iminophosphoranes on gram scale (in batch and flow), mechanistic studies of this new transformation, and applications of these new iminophosphoranes as ligands in nickel catalysis under thermal, electrochemical, and photochemical conditions.

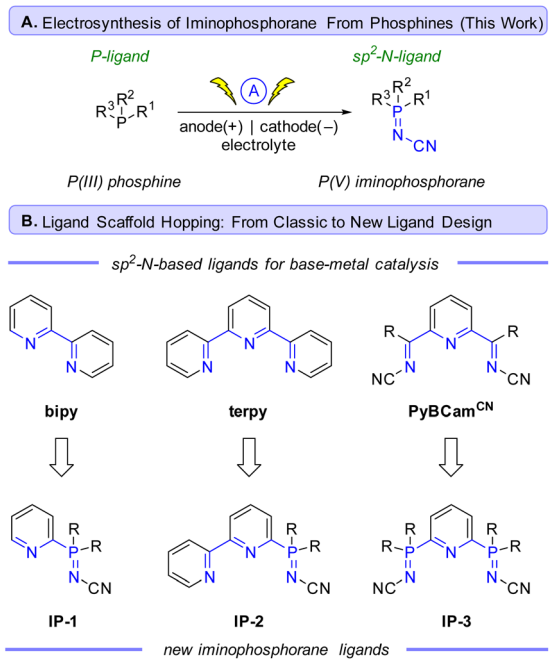


Scheme 2 (A) Electrosynthesis of iminophosphoranes from phosphines. (B) Ligand scaffold hopping.

## Results and discussion

### Reaction optimization

Inspired by the success of the *N*-cyano imine ligands (*i.e.* pyridine-2,6-bis(*N*-cyanocarboxamidine), PyBCam$^{CN}$) reported by Weix and Hansen for nickel-catalyzed cross-electrophile couplings (Scheme 2B),[31] we chose to focus on *N*-cyano iminophosphoranes (Scheme 2A) for our initial explorations. Specifically, we targeted iminophosphorane **1a** (Scheme 3) for the reaction development as it is air-stable and has a UV-vis chromophore, thus enabling analysis of reaction mixture *via* UPLC.

Given that the modified Kirsanov reaction uses $Br_2$ to oxidize $PPh_3$ to $Ph_3PBr_2$ followed by amination to access iminophosphoranes,[11] we explored using bromide-containing electrolytes to effect an anodic generation of $Br_2$ to mediate the oxidation of $Ph_3P$ (**2a**) in the presence of cyanamide (**3**) (Scheme 3A). The use of $Et_4NBr$ as an electrolyte enabled oxidation of $PPh_3$ in 4 : 1 (v/v) MeCN/MeOH provided 15% yield of **1a** when using a graphite anode, a stainless-steel cathode along with guanidine **4** in 12%

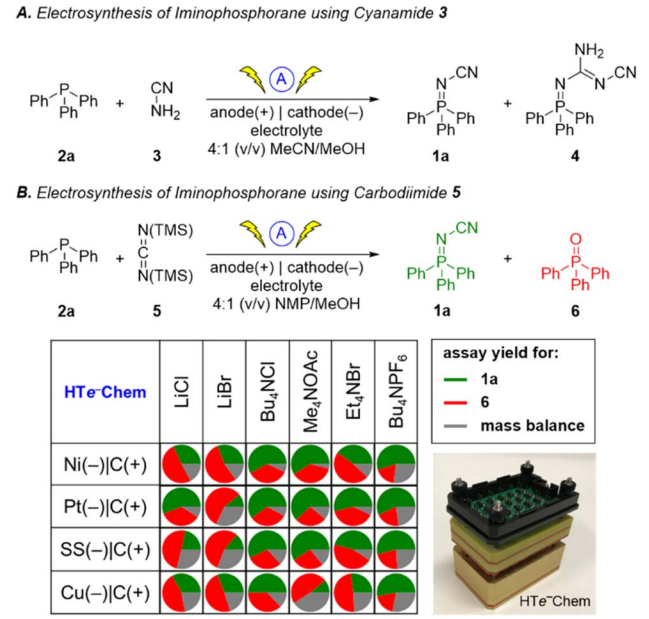


Scheme 3 (A) Initial attempts at synthesizing iminophosphorane **1a** using cyanamide. (B) Heat map of assay yields obtained using HTe⁻Chem to screen electrolytes and electrode for the synthesis of iminophosphorane **1a** using bis(trimethylsilyl)carbodiimide. Conditions: 30 μmol scale (0.1 M) using constant current (1 mA) using 2 F $mol^{-1}$ charge at room temperature (Note: C = graphite, SS = stainless steel).

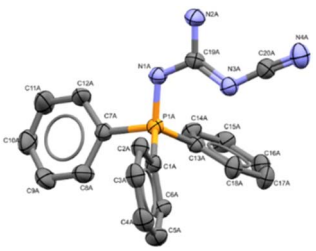

Fig. 1 X-ray crystallographic structure of side-product **4** (CCDC 2259467). ORTEP ellipsoid plotted at 50% probability.

yield. The structure of **4** was confirmed by X-ray crystallography (Fig. 1).

We explored an alternative aminating reagent towards improving the selectivity for iminophosphorane **1a** over guanidine **4**. We wondered whether bis(trimethylsilyl)carbodiimide (**5**) could provide a more soluble surrogate of cyanamide towards improving the outcome of the reaction. Indeed, the use of **5** under otherwise identical conditions provided iminophosphorane **1a** in 70% yield and no detectable guanidine **4**. We explored these conditions with a handful of other phosphines but soon realized that the solubility of the phosphine starting material was poor in a number of examples (*e.g.* xanthphos).

Thus, we replaced MeCN with NMP as a cosolvent to achieve improved solubility, however the yield for **1a** dropped to 43%. Given the multivariate nature of this optimization problem, we turned to high-throughput experimentation to address this challenge. Using the recently reported[32] and commercialized[33] HTe⁻Chem reactor, we explored both electrolyte and electrode variables using 4 : 1 (v/v) NMP/MeOH as the solvent system (Scheme 3B). The use of $Me_4NOAc$ as the electrolyte in combination with platinum cathode and graphite anode provided the highest yield of iminophosphorane **1a**. The $Ph_3P{=}O$ (**6**) side product was postulated to arise from adventitious water or oxygen in the reaction mixture reacting competitively against the aminating reagent.[34]

Based on reaction optimization using the HTe⁻Chem reactor, the optimal conditions were translated from 30 μmol scale to the Electrasyn 2.0 setup on 2 mmol scale using a current of 10 mA ($j$ = 4.2 $cm^2$ $mA^{-1}$) and a charge of 2.5 F $mol^{-1}$. The choice of NMP and $Me_4NOAc$ also facilitated reaction workup, as the reaction could be poured into water to precipitate out the desired product in many cases while leaving the electrolyte in solution. Collection of the crude product *via* filtration followed by recrystallization or column chromatography afforded the desired products in high purity with a variety of substrates (see ESI† for details).

## Substrate scope

With optimal reaction conditions in hand, we turned our attention to exploring the substrate scope of our electrochemical synthesis of iminophosphoranes (Table 1). We targeted a diverse substrate scope, drawing inspiration from commercially available phosphine ligands commonly used in transition-metal catalysis (*e.g.*, cross-couplings). Amination of triphenylphosphine on 2 mmol scale provide **1a** in 83% yield. Electronically varied triarylphosphines are well tolerated as demonstrated with *para*-substituted analogues of triphenylphosphine: *p*-OMe (**7**) 74% yield, *p*-F (**8**) 92% yield, *p*-Cl (**9**) 73% yield, and *p*-$CF_3$ (**10**) 83% yield. Styrenyl containing product **11** is obtained in 79% yield, which could have application as a precursor to iminophosphorane-functionalized polystyrene materials (*e.g.* polystyrene resin-bound ligand/catalyst for heterogenous catalysis).[35] *Ortho*-substitution is well tolerated as demonstrated by being able to access product **12** in 86% yield. Even tertiary amines functionalized phosphine can be carried through the reaction, albeit in diminished yield, as exemplified with an analogue of $Ph_2$-APhos to access **13** in 39% yield.

Arylalkylphosphines are also suitable substrates, as iminophosphorane **14** is accessed in 56% yield from diphenylcyclohexylphosphine. Conversion of dicyclohexylphenylphosphine to **15** is achieved in high yield (82%). The conversion of CyJohnPhos to **16** in 75% yield demonstrates that an *ortho*-aryl substituent on the phenyl ring is tolerated with these dialkylmonoarylphoshine substrates. Acetals can be carried through this transformation as showcased with the functionalization of the $^{me}$CgPPh ligand to product **17** in 89% yield. Trialkylphosphines are also suitable as demonstrated by the use of tribenzylphosphine to access **18**, although a diminished yield was observed.

Heterocycles can also be brought through this transformation to access iminophosphorane products, potentially

Table 1 Reaction scope for the electrosynthesis of iminophosphorane using an IKA ElectraSyn 2.0[a]

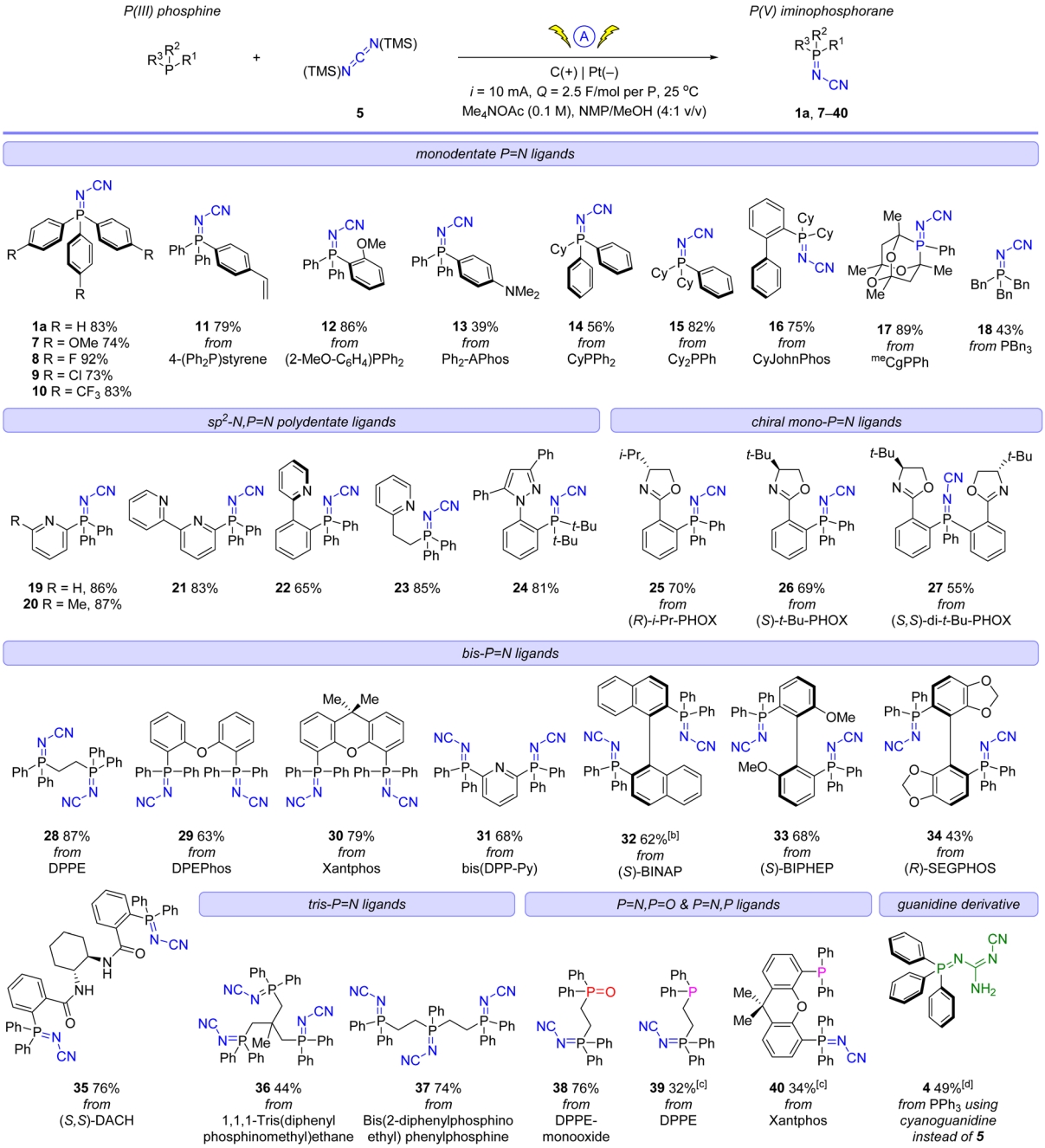


[a] Standard condition: 2.0 mmol of phosphine (0.13 M) in 4 : 1 v/v NMP/MeOH containing **5** (6.0 mmol of per phosphorus), and 1.5 mmol of $Me_4NOAc$; constant current electrolysis (10 mA, $j$ = 4.2 mA $cm^{-2}$) and a charge of 2.5 F $mol^{-1}$ per phosphorus using a graphite anode and a platinum foil cathode. [b] 1 mmol of phosphine (0.07 M) using 14 : 1 v/v NMP/MeOH containing 1.5 mmol of $Me_4NOAc$. [c] Same as standard conditions, except 6.0 mmol of **5** was used and the charge was 2.5 F $mol^{-1}$. [d] Same as standard conditions, except 6.0 mmol of *N*-cyanoguanidine was used instead of **5**.

providing bidentate functionality, as demonstrated with products (**19–23**). The incorporation of pyridyl fragments is exemplified with both triaryl and diarylphosphines with products **19** (86% yield), **20** (87% yield), **21** (83% yield), **22** (65%), and **23** (85% yield), while access to a pyrazole-containing ligand is demonstrated with product **24** (81% yield). Chiral phosphine ligands, such as those based on phosphinooxazolines (PHOX) substructures, can be transformed to their corresponding iminophosphoranes. This was exemplified with products **25–27** that were obtained in yields ranging from 55–70%, without evidence of ee erosion.

The bidendate phosphines DPPE, DPEPhos, and Xantphos provide **28–30** in 87%, 63%, and 79% yield, respectively. 2,6-Bis(diphenylphosphino)pyridine is used to make **31** in 68%

yield, providing a tridentate ligand[36] based on three $sp^2$-nitrogens. The privileged chiral ligand[37] BINAP is converted to its iminophosphorane analog **32** in 62% yield. Similarly, popular BIPHEP and SEGPHOS ligand scaffolds are used to access **33** and **34** in 68% and 43% yields, respectively. The bis-amide containing Trost ligand[38] (*S*,*S*)-DACH could be converted to the corresponding bis-iminophosphorane **35** in 76% yield.

Tripodal ligands are useful in coordination chemistry and catalysis. We explored the use of commercially available tridentate "triphos"[39] ligands which enabled access to tris(iminophosphorane) ligands **36** and **37** in 44% and 74% yield, respectively. These ligands are envisioned to be useful for tripodal complex formation, a strategy that is often used with first-row transition metals.[40]

Access to hetero-bis-phosphine derivatives was explored as illustrated with products **38–40**. Two strategies were utilized depending on the target: (1) starting from bis-phosphine monooxides, or (2) passing slightly more charge (*i.e.* 2.5 F $mol^{-1}$) than the theoretical minimum charge of 2 F $mol^{-1}$ to oxidize one of the two phosphines. Mixed P=O,P=N ligand **38** was accessed starting from the commercially available DPPE-mono-oxide (*i.e.* P(III)–P(V) monoxide). In contrast, mixed P(III)–P(V) DPPE structures **39** and **40** were obtained by passing only 2.5 F $mol^{-1}$ of charge under otherwise identical conditions to those employed in Table 1. Selectivity between mono- and bis-oxidation products is challenging and is the cause of the lower yields for substrates **39** and **40**. For example, bis oxidation to **28** is observed in *ca.* 40% yield after 2.5 F $mol^{-1}$ when synthesizing **39**. The ESI† contains additional substrates that were attempted but provide low yield or no product. Limitations include the use of electron-rich phosphines like trialkylphosphites, triphenylphosphites, although trialkylphosphines are suitable (see the ESI† for details).

Finally, returning to the side-product **4** that was obtained during the reaction optimization work, we wondered whether inexpensive *N*-cyanoguanidine, commonly used as a fertilizer,[41] could be utilized in our reaction as the aminating reagent. Gratifyingly, the formation of iminophosphorane **4** containing cyanoguanidine was achieved in 49% yield.

The iminophosphoranes in Table 1 were isolated by either precipitation from the crude reaction mixture using water as an anti-solvent or *via* an aqueous workup, and in numerous cases a subsequent purification step *via* silica gel column chromatography, all in the presence of air. This highlights their air stability and resistance to hydrolysis. This is in contrast to *N*-alkyl substituted iminophosphoranes, which can be susceptible to decomposition to the corresponding phosphine oxide (*e.g.* Staudinger ligation).[22]

## Reaction mechanism

In order to gain mechanistic insight into the reaction, we conducted DFT calculations and followed up with a series of experiments based on NMR spectroscopy ($^1$H, $^{13}$C, $^{31}$P) and cyclic voltammetry. Five potential mechanisms were initially considered (See ESI† Scheme S2 along with associated discussion). Based on the data from these studies, a proposed mechanism is illustrated in Scheme 4. Reduction of methanol at the cathode generates hydrogen and methoxide. The methoxide attacks diimide **5**, which upon loss of TMS–OMe (**41**) generates anion **42**. Oxidization of **42** leads to *N*-centered radical **43**. Subsequent attack of phosphine (**2**) generates **44** (ref. 42) which is immediately oxidized to **45**. Generation of a second equivalent of methoxide, analogous to above, enables breakdown of **45** to generate the desired iminophosphorane product **46** and a second equivalent of TMS–OMe (**41**). To the best of our knowledge this represents a rare example of a domino electrolysis reaction,[43,44] which could be categorized as a sequential paired electrolysis followed by a convergent paired electrolysis.[30a,45]

## Ligand properties

To gain insight into electronic effects of modifying P(III) ligands into their analogous P(V) structures (various iminophosphoranes and phosphine oxide), we computed their frontier molecular orbitals using M06-2X/6-31+G(d) SMD = MeCN. Fig. 2 illustrates the HOMO and LUMO orbitals for $Ph_3P$ (**2a**), $Ph_3P$=N–CN (**1a**), $Ph_3P$=N–Ph (**47**), $Ph_3P$=N–Me (**48**), $Ph_3P$=N–H (**49**), and $Ph_3P$=O (**6**). The HOMO energy decreases monotonically across the following series: −7.05 eV ($Ph_3P$=N-Ph), −7.31 eV (Ph3P), −7.34 eV ($Ph_3P$=N–Me), −7.73 eV (Ph3P=N–H), −8.13 eV ($Ph_3P$=N–CN), −8.48 eV ($Ph_3P$=O); all values are *versus* vacuum. Across the series of iminophosphoranes in Fig. 2, *N*-cyano iminophosphorane **1a** has the lowest lying HOMO and thus should be the most oxidatively resistant from the series and is in consistent the observation that it is air-stable. The DFT calculations show the HOMO is destabilized in the *N*-cyano iminophosphoranes compared to the analogous phosphine oxide, suggesting stronger σ-donor ability, yet still weaker than the analogous P(III) ligand. The LUMO energies do

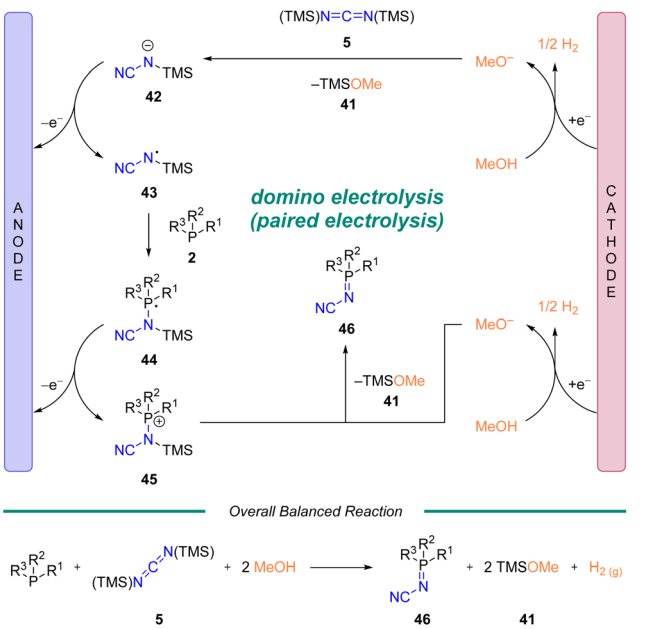


Scheme 4 Proposed mechanism of domino-electrolysis.

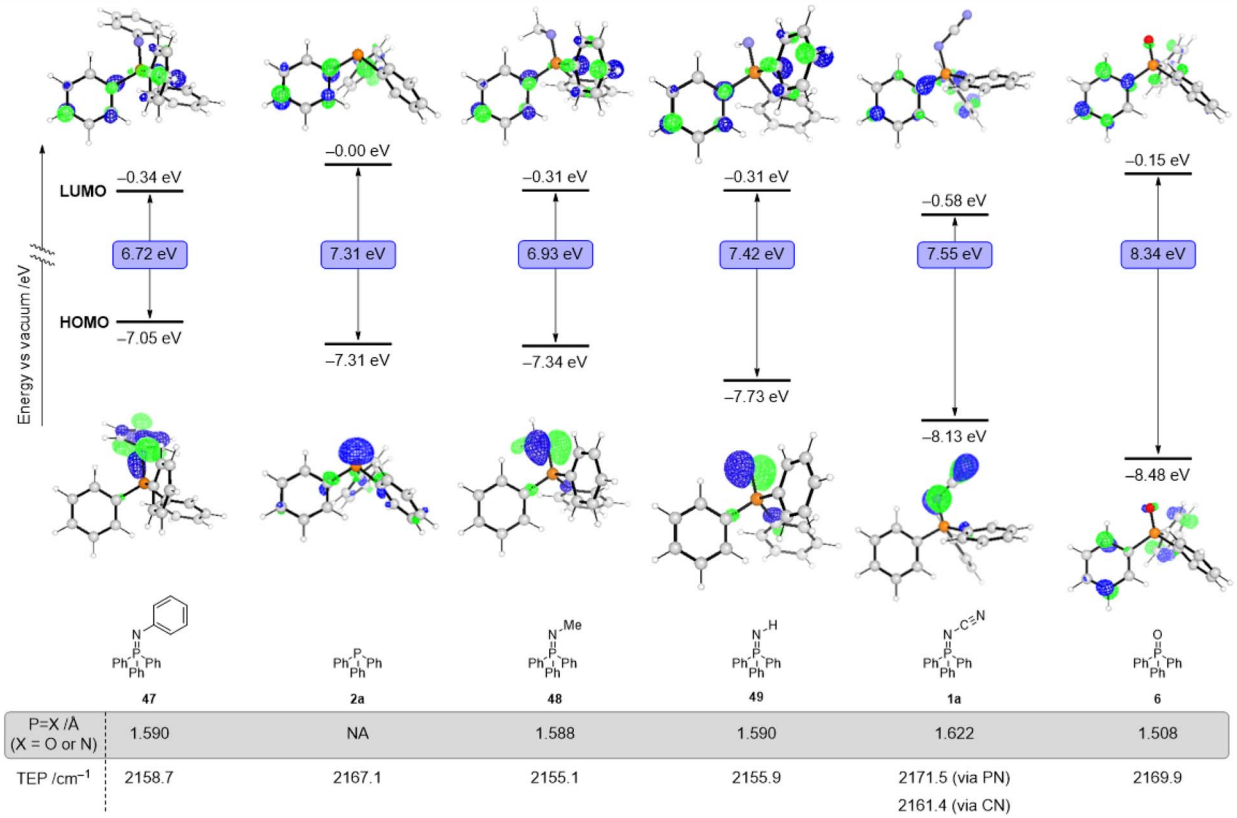


Fig. 2 DFT computed lowest unoccupied molecular orbital (LUMO), (top) and highest occupied molecular orbital (HOMO) (bottom) for various P(III) and P(V) ligands using M06-2X/6-31+G(d) SMD = MeCN (note: orbitals are plotted using isolvalue = 0.075 a.u.) along with P = X (X = O or N) bond lengths. Tolman electronic parameters obtained from DFT calculations using MPW1PW91 functional and the following basis sets: 6-311+G(2d) for Ni and 6-311+G(d,p) for all other atoms.

not decrease monotonically when considering the ligands in the same order as above, specifically the LUMO energy varies as follows: −0.01 eV ($Ph_3P$), −0.34 eV ($Ph_3P$=N–Ph), −0.01 eV ($Ph_3P$), −0.31 eV ($Ph_3P$=N–Me), −0.31 eV ($Ph_3P$=N–H), −0.58 eV ($Ph_3P$=N–CN), and −0.15 eV ($Ph_3P$=O). Overall, these changes highlight that formal oxidation of the P(III) ligands to P(V) results not only in significant electronic changes, but also that these changes may be different depending on which group is attached to the P(V) centre (O for a phosphine oxide or various N–R groups for the various iminophosphoranes). Experimental study of the reduction potential across a subset of the iminophosphoranes using cyclic voltammetry reveals that these ligands are redox active (Fig. 3). Reversible reduction is observed for *N*-cyano iminophosphoranes, such as pyridyl containing ligand **19** ($E_{red}$ = −2.45 V *vs.* $Fc/Fc^+$) and bipyridyl based ligands **21** ($E_{red}$ = −2.34 V *vs.* $Fc/Fc^+$), but not triphenylphosphine based *N*-phenyl iminophosphorane **47** ($E_{p1/2,red}$ = −2.97 V *vs.* $Fc/Fc^+$), nor *N*-cyano iminophosphorane **1a** ($E_{p1/2,red}$ = −2.79 V *vs.* $Fc/Fc^+$). Bis-iminophosphorane functionalized pyridine ligands **31** exhibits two sequential reduction events: ($E_{p1/2,red}$ = −2.06 V and −2.22 V *vs.* $Fc/Fc^+$), each is quasi-reversible. The redox active nature of these ligands may be beneficial for catalytic applications where reduction events are taking place (*e.g.* metal catalysed reductive cross-couplings).

We also calculated the Tolman electronic parameter (TEP) to characterize the electronic properties of these ligands (Fig. 2).[46–48] The TEP for a ligand L, which is defined as the IR frequency associated with the $A_1$ stretch of the CO groups of the $Ni(CO)_3L$ complex, correlates with the electron-donating ability of the ligand. The computed TEP value of $Ph_3P$=N–CN (**1a**) for

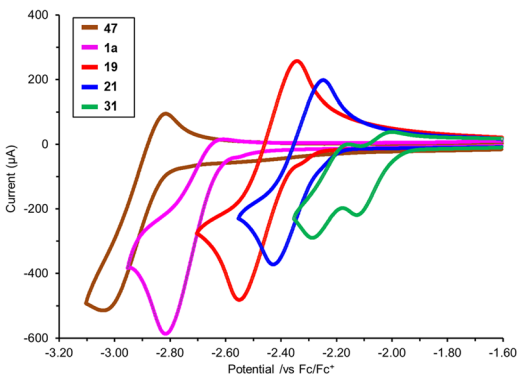


Fig. 3 Cyclic voltammetry of selected iminophosphoranes illustrating their redox active properties. Data measured from 10 mM solutions of analyte in 0.1 M $Bu_4NPF_6$ in MeCN using a glassy carbon working electrode, a Pt counter electrode, a reference electrode comprised of a Ag wire in 10 mM $AgNO_3$ in 0.1 M $Bu_4NPF_6$ in MeCN ($\nu$ = 500 mV $s^{-1}$).

binding *via* the nitrogen of the P=N moiety is higher (2171.5 $cm^{-1}$) than the TEP values of $Ph_3P$=N–Ph (2158.7 $cm^{-1}$) and $Ph_3P$=N–Me (2155.1 $cm^{-1}$), supporting our proposal that *N*-cyano iminophosphoranes are more electron-deficient than *N*-aryl or *N*-alkyl iminophosphoranes.

To probe structural aspects of these new iminophosphoranes, a number of ligands (**13**, **24**, (*R*)-**25**, **28**, **29**, (*S*)-**33**, **38**, and **39**), were crystallized and characterized by X-ray crystallography (Fig. 4).[49] Key structural parameters are summarized in the ESI† (see Table S11). The bent geometry of the "P=N–CN" fragment was confirmed with a typical bond angle associated with the P=N–C fragment being *ca.* 124°. The iminophosphorane **4**, (*R*)-**25**, **28**, **29**, **38** and **39** have comparable P=N bond lengths to $Ph_3P$=N–Ph (1.603 Å), see ESI.†

A more detailed comparison of bond metrics is provided in the ESI,† including comparison with X-ray crystallographic structures in the Cambridge Structural Database. The crystal structure of iminophosphorane (*R*)-**25** and (*S*)-**33** confirmed that the absolute configuration of the chiral starting materials was retained in our electrochemical synthesis.

To learn about the coordination geometry *N*-cyano iminophosphoranes, we grew single crystals from *ca.* 3 : 1 (v/v) MeCN/MeOH solutions of ligand **21** in the presence of $NiBr_2 \cdot 3H_2O$ using $Et_2O$ vapour diffusion. The X-ray crystallographic structure obtained was nickel complex **Ni-1** (Fig. 5) which is a tetranuclear complex, where each Ni has octahedral coordination geometry (Fig. 5B). Both $sp^2$-*N* of the 2,2′-bipyridine moiety and the nitrogen of the P=N fragment of the iminophosphorane coordinate to Ni. The nitrile nitrogen of the iminophosphorane coordinates to a neighboring Ni atom in a cyclic tetrameric arrangement. Additional coordination sites on the Ni are occupied by bromide and methanol (where the occupancy is split 75%/25% between these two ligands as shown in Fig. 5).

The fact that either nitrogen of the *N*-cyano iminophsphorane can participate in coordination to metals is consistent with previous coordination complexes of $Ph_3P$=N–CN with Pt and Pd.[50] Coordination of Ni to *N*-aryl iminophosphorane has also been documented.[51] The ambidentate nature of *N*-cyano iminophsphoranes is characterized by the computed TEP values shown in Fig. 2 which highlight the nitrogen of the C≡N moiety is more electron donating (TEP = 2161.4 $cm^{-1}$) than the nitrogen of the P=N moiety (2171.5 $cm^{-1}$).

## Application to catalysis

To demonstrate the utility of the iminophosphorane ligands, we chose to explore five types of Ni-catalysed cross-coupling reactions which are reshaping how chemists synthesize molecules in industry (Scheme 5 and 6), specifically, both a thermally and an electrochemically driven $C(sp^2)$–$C(sp^3)$ cross-electrophile coupling (XEC), a thermally activated $C(sp^2)$–$C(sp^2)$ XEC, a photochemical arylative C–H functionalization, and a site-selective C–N coupling using electrochemistry.

The groups of Weix,[52] Hansen,[52b,53] and Sevov,[54] Reisman,[55] amongst others,[56] have each contributed notable advances in Ni-catalysed XEC beyond the early work by Périchon.[57] These recent reports typically feature the use of two ligand systems (*e.g.* a bipyridine and a terpyridine ligand) and their relative ratio can be critical to the success of the reaction outcome.[52b] Recent works by Weix,[52d] Martin,[58] Sigman and Doyle[59] as well as others,[60] have highlighted the importance of ligands that can stabilize Ni(I) catalytic intermediates. We sought to evaluate the usefulness of these *N*-cyano iminophosphoranes in XECs.[52b]

Scheme 5 reports a high throughput experimentation screen of 12 ligands for a nickel-catalyzed XEC between 4-(4-bromophenyl)morpholine (**50**) and 3-bromobutanenitrile (**51**) at 0 °C using Zn dust at the terminal reductant. The 12 ligands screened consisted of 4′-di-*tert*-butyl-2,2′-dipyridyl (**dtbbpy**) and 11 different *N*-cyano iminophosphoranes. The top three performing ligands were *N*-cyano iminophosphorane ligands **35** (derived from (*S*,*S*)-DACH), ligand **28** (based on DPPE), and ligands **37** (based on unsymmetrical triphos), providing assay yields of 76%, 65%, and 54%, respectively. A 1 mmol scale up of

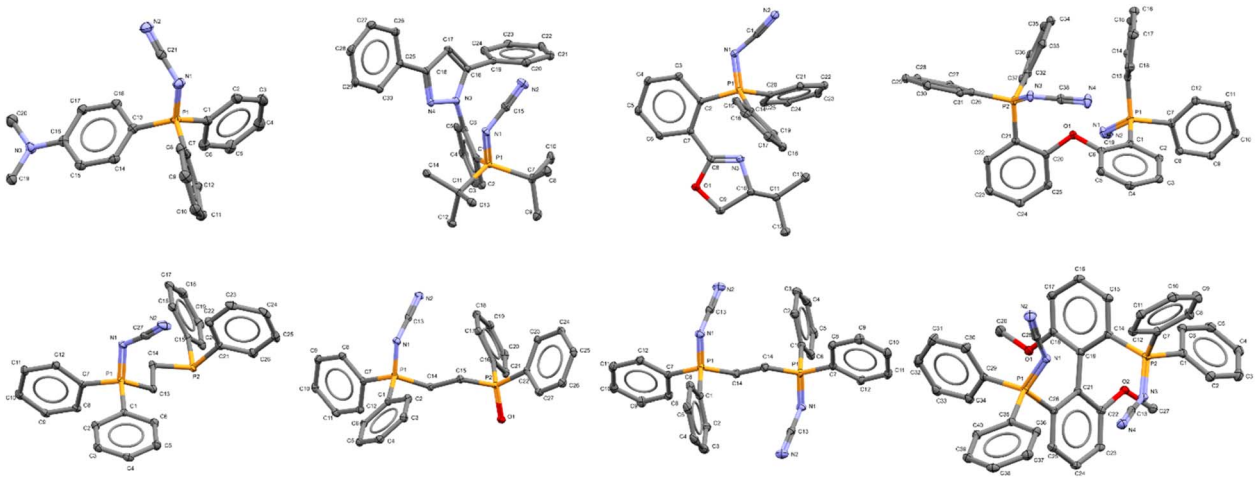

Fig. 4 X-ray crystallographic structure of iminophosphorane, (top row, left to right): **13** (CCDC 2258974), **24** (CCDC 2258975), (*R*)-**25** (CCDC 2259466), **29** (CCDC 2258980); (bottom row, left to right): **39** (CCDC 2258979), **38** (one of two inequivalent geometries, CCDC 2258978), **28** (CCDC 2258976), and (*S*)-**33** (CCDC 2258977) (Note ORTEP ellipsoid plotted at 50% probability).

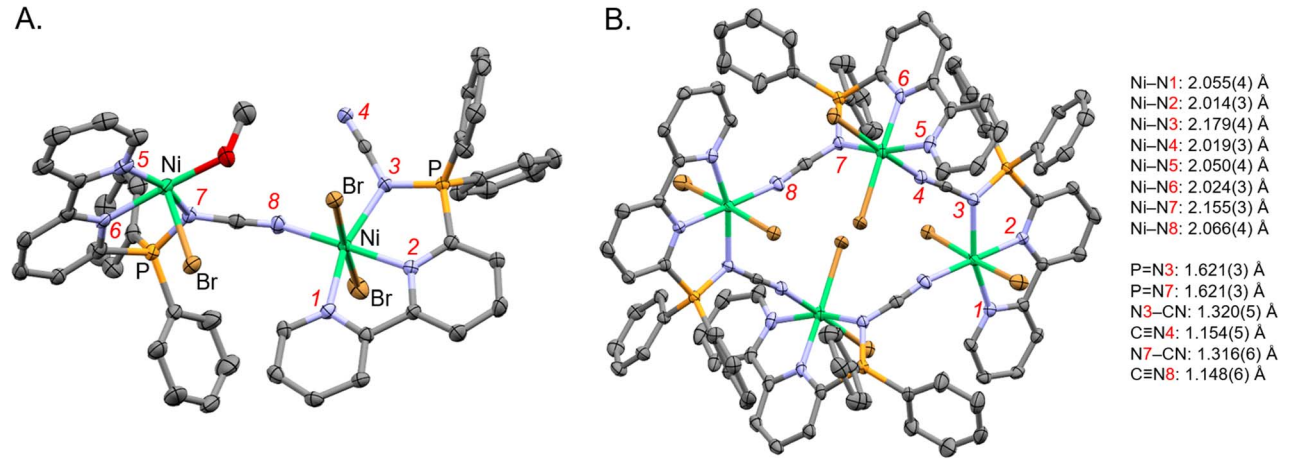


Fig. 5 X-ray crystallographic structure of nickel complex **Ni-1** (CCDC-2329725). (A) A subunit of **Ni-1** illustrating that both Ni bound to both $sp^2$-*N* of bipyridine and the N of the P═N unit of ligand **21** (minor part with methanol coordinating to the nickel center shown). (B) The tetranuclear arrangement of **Ni-1** (minor methanol motif omitted and major bromine part shown). Hydrogen atoms, non-coordinative counter ions, solvent, and minor parts (by occupancy) omitted for clarity. Thermal ellipsoids given at the 50% probability level. Color code: grey (carbon), red (oxygen), blue (nitrogen), green (nickel), orange (phosphorus), brown (bromine).

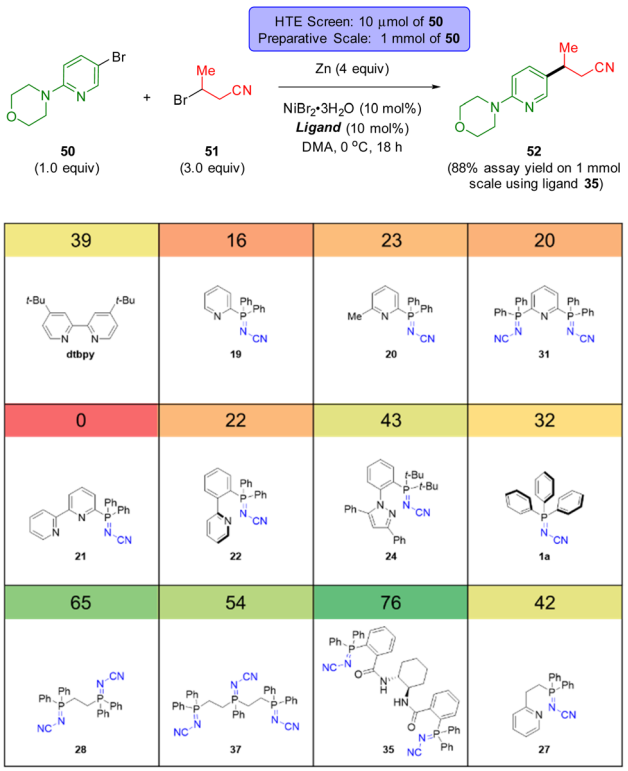


Scheme 5 HTE screen (10 μmol scale based on **50**) of $sp^2$-*N*-based ligands in a thermal $C(sp^2)$–$C(sp^3)$ XEC coupling. The number in the coloured box above each ligand is the assay yield for **52**.

this XEC reaction using ligands **33** provided an assay yield of 88% yield.

Scheme 6A reports our results in exploring an electrochemically-driven $C(sp^2)$–$C(sp^3)$ cross-electrophile coupling of ethyl 4-bromobenzoate (**52**) and 3-bromobutanenitrile (**51**) to access **53**. The yield of desired XEC product **53** is tabulated in Scheme 6A along with key hydrodehalogenation impurity **54** and homocoupling side-product **55**. We chose to focus our initial explorations using polydentate iminophosphorane ligands as described by our inspiration illustrated in Scheme 2 and the success of polydentate $sp^2$-*N*-based ligands like 4,4′-di-*tert*-butyl-2,2′-dipyridyl (**dtbbpy**) or 4″-tri-*tert*-butyl-2,2′:6′,2″-terpyridine (**ttbtpy**) in Ni-catalysis. After testing a selection of polydentate iminophosphorane ligands (**28**, **31**, **35**, **37**), we were delighted to obtain a high yield of product **53** with iminophosphorane ligands **31** and **37**. The best-performing ligand was **37** providing 90% yield of XEC product **53** with, while minimizing impurities **54** and **55** to 3% and 6%, respectively. In comparison, the use of **dtbbpy** or **ttbtpy** on their own provided lower yields of 73% and 30% respectively.

Noteworthy, the use of the P(III) ligand **DPPE** provided only 3% yield of the XEC product **53** and the reaction mixture contained no evidence of **DPPE** at the end of the reaction, but instead the bis-oxide analog of DPPE was observed. Control experiments using the mono-oxide of DPPE (**DPPEO**) (or other bis-oxide ligands, see ESI† for details) as the ligand in the cross-electrophile coupling of **51** and **52** did not provide meaningful amounts of product **53**. Specifically, **53** was obtained in 13% using **DPPEO**. This highlights why the P(V) iminophosphorane ligands are more suitable as they are less prone to oxidative decomposition pathways, unlike air/moisture-sensitive P(III) ligands, while also providing good catalytic activity unlike phosphine oxides.

$sp^2$–$sp^2$ XECs are also of interest as an alternative to Suzuki cross-couplings, bypassing the need for boronic acids which can be prone to protodeboronation.[60] Weix has reported a dual catalytic system using nickel and palladium-catalysis to cross-couple aryl bromides with aryl triflates to access biaryls using Zn dust as the reductant.[61] Employing this strategy, we successfully demonstrate that ligand **21** can enable the $sp^2$–$sp^2$ cross coupling of aryl bromide **50** with aryl triflate **56** to access product **57** in 64% yield (Scheme 6B).

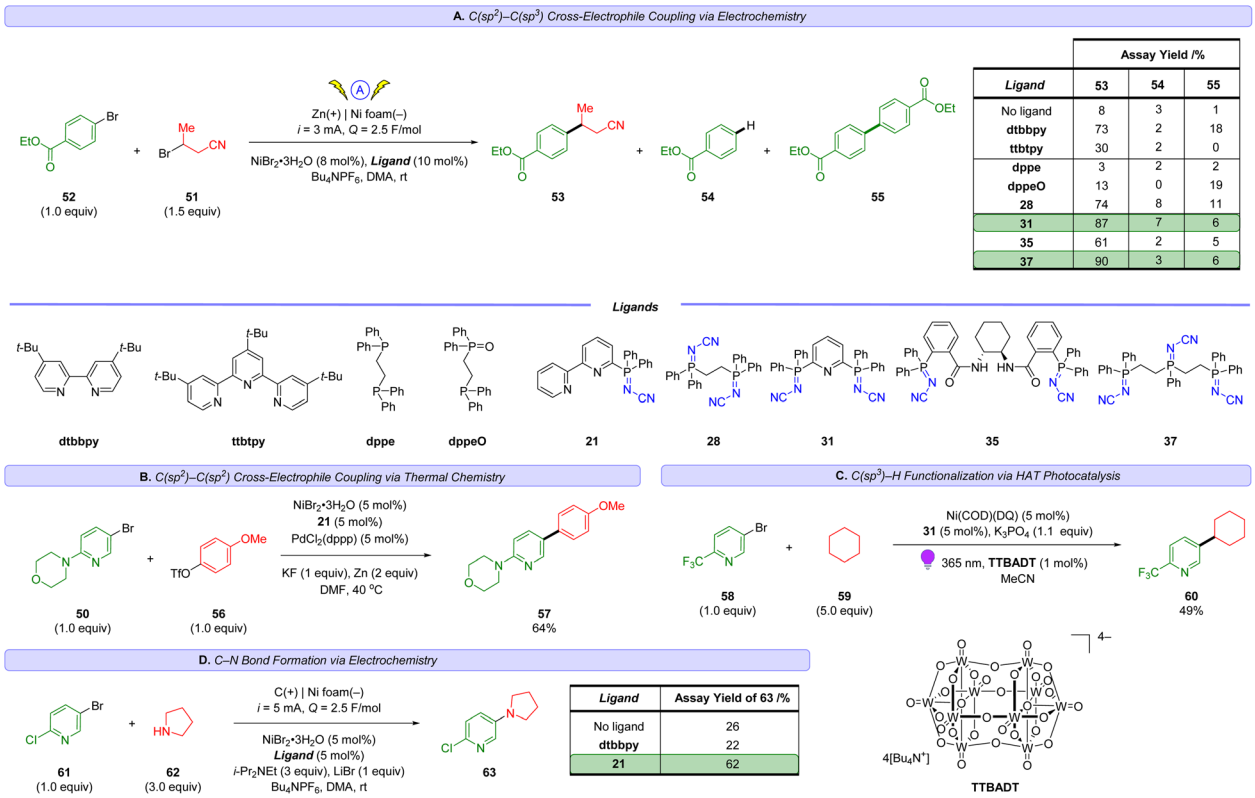


Scheme 6 Application of iminophosphoranes in a nickel-catalyzed reactions: (A) C($sp^2$)–C($sp^3$) cross-electrophile coupling *via* electrochemistry, (B) C($sp^2$)–C($sp^2$) cross-electrophile coupling *via* thermal chemistry, (C) C–N coupling reaction using electrochemistry, and (D) C–H functionalization using HAT photocatalysis.

To gain insight into the viability of using iminophosphorane ligands in high energy photochemical conditions (365 nm) with open shell species generated *via* hydrogen atom transfer (HAT) catalysis, we explored the use of MacMillan's metallaphotoredox method[62] for direct arylation of C($sp^3$)–H bonds (Scheme 6C). Gratifyingly, irradiation of mixtures containing 2-trifluoromethyl-5-bromopyridine (**58**) and cyclohexane (**59**) in the presence of tetrakis(tetrabutylammonium)decatungstate ($(n\text{-}Bu_4N)_4[W_{10}O_{32}]$, **TTBADT**), Ni(COD)(DQ)[63] and iminophosphorane **31** with 365 nm provided the desired product **60** in useful yields.

Electrochemical Ni-catalyzed C–N cross couplings can offer milder conditions over their thermal counterpart (*e.g.* 20 °C instead of >110 °C).[64] We explored the application of several iminophosphorane ligands (see ESI† for details) in the context of coupling aryl halide **61** with pyrrolidine (**62**) to access **63** (Scheme 6D) using electrochemical Ni-catalyzed conditions similar to those developed by Baran and coworkers.[65] Gratifyingly, we obtained site selective coupling (Br over the activated Cl) to product **63** in 62% yield (and less than 5% yield of the product associated with C–N coupling at the 2-chloro position was observed). Interestingly, **dtbbpy** performed poorly for this substrate (22% yield of **58**), further highlighting the importance of expanding the diversity of $sp^2$-*N*-ligands towards improving selective cross-coupling reactions.

To demonstrate the scalability of the electrochemical synthesis of iminophosphoranes, we translated our batch electrosynthetic conditions to flow conditions (Scheme 7). Utilizing a parallel plate reactor equipped with carbon felt on graphite as the anode and a Pt cathode, we operated this flow electrolysis reactor in recirculating mode. By switching the electrolyte from $Me_4NOAc$ to the more soluble $Bu_4NOAc$, and

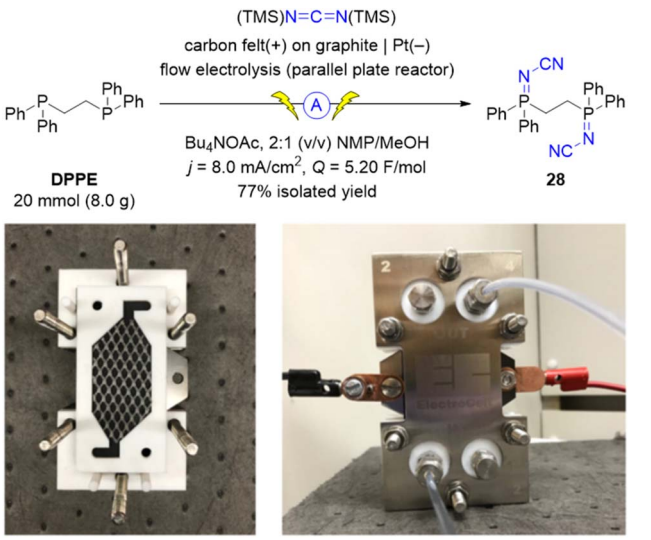


Scheme 7 Multi-gram-scale flow-electrosynthesis of ligand **28** using an ElectroCell Micro Flow Cell® parallel plate reactor. Photographs illustrate the partially and fully assembled reactor.

using carbon felt on graphite as the anode instead of graphite (increasing the surface area), we were able to increase the current density from 4.2 to 8.0 mA $cm^{-2}$, and ultimately increase productivity. The use of 5.20 F $mol^{-1}$ of charge provided complete consumption of both the starting material (**DPPE**) and the P(III)–P(V)-intermediate **39**. The crude reaction mixture was simply diluted with water to induce a direct crystallization from the reaction mixture to isolate **28** (77% isolated yield, corrected for purity).

## Conclusions

We have developed an operationally simple and safe electrochemical synthesis of new iminophosphorane ligands from commercially available phosphines.[66] A paired-electrolysis mechanism is operational where an electrogenerated base[67] triggers the formation of a key intermediate to enable a rare example of domino electrolysis. This synthetic method is safer than conventional Staudinger chemistry (herein we would have required the use of cyanogen-azide, NC–$N_3$, which is extremely hazardous due to its energetic nature, in fact it is a primary explosive).[68] The utility of these compounds as ligands was demonstrated in five Ni-catalyzed cross-couplings, including $C(sp^2)$–$C(sp^3)$ and $C(sp^2)$–$C(sp^2)$ cross-electrophile couplings. Improved yields for the XEC of ethyl 4-bromobenzoate with 3-bromobutanenitrile were obtained when using iminophosphorane **31** or **37** compared to the commonly used **dtbbpy** and **ttbtpy**. Iminophosphorane ligand **21** also enabled site selectivity in a C–N coupling of a polyhalogenated pyridine derivative. This highlights the need of a diverse library of ligands to screen whenever optimizing for yields and selectivity in catalytic reactions. We anticipate broad applicability of these ligands for transition metal catalysis where $sp^2$-nitrogen based ligands have traditionally been used (*e.g.* C–N, C–O, C–C cross-couplings). Applications of this electrosynthetic method to access iminophosphorane organocatalysts for anion-binding is also envisioned.[20]

## Data availability

The ESI† contains the data associated with this article.

## Author contributions

D. L. conceived the project. V. M., D. L., and Y.-h. L. directed the project. All the authors performed experiments. The manuscript was written through contributions of all authors.

## Conflicts of interest

There are no conflicts to declare.

## Acknowledgements

V. M. and M. T. C. acknowledge support from the Postdoctoral Fellowship program at Merck & Co., Inc., Rahway, NJ, USA. We acknowledge Ryan Cohen and Mikhail Reibarkh for assistance with the $^{13}C\{^1H,^{31}P\}$ NMR experiment for ligand **28**. We thank François Lévesque, Charles Yeung, and Eric Phillips (all at Merck & Co., Inc., Rahway, NJ, USA) for insightful discussions and feedback.

## Notes and references

1 (*a*) A. L. Clevenger, R. M. Stolley, J. Aderibigbe and J. Louie, *Chem. Rev.*, 2020, **120**, 6124–6196; (*b*) M. B. Smith, Phosphorus Ligands, *Reference Module in Chemistry, Molecular Sciences and Chemical Engineering*, 2013, DOI: 10.1016/B978-0-12-409547-2.01037-4; (*c*) E. I. Musina, A. S. Balueva and A. A. Karasik, Tertiary Phosphines: Preparation, in *Organophosphorus Chemistry*, 2022, vol. 51, pp. 1–61, DOI: 10.1039/9781839166198-00001.
2 H. Guo, Y. C. Fan, Z. Sun, Y. Wu and O. Kwon, *Chem. Rev.*, 2018, **118**, 10049–10293.
3 D. Parmar, S. Raja and M. Rueping, *Chem. Rev.*, 2014, **114**, 9047–9153.
4 (*a*) H. Li, K. M. Belyk, J. Yin, Q. Chen, A. Hyde, Y. Ji, S. Oliver, M. T. Tudge, L.-C. Campeau and K. R. Campos, *J. Am. Chem. Soc.*, 2015, **137**, 13728–13731; (*b*) Y. Ji, H. Li, A. M. Hyde, Q. Chen, K. M. Belyk, K. W. Lexa, J. Yin, E. C. Sherer, R. T. Williamson, A. Brunskill, S. Ren, L. C. Campeau, I. W. Davies and R. T. Ruck, *Chem. Sci.*, 2017, **8**, 2841–2851.
5 (*a*) Y. Ji, E. P. Plata, C. S. Regens, M. Hay, M. Schmidt, T. Razler, Y. Qiu, P. Geng, Y. Hsiao, T. Rosner, M. D. Eastgate and D. G. Blackmond, *J. Am. Chem. Soc.*, 2015, **137**, 13272–13281; (*b*) R. J. Fox, N. L. Cuniere, L. Bakrania, C. Wei, N. A. Strotman, M. Hay, D. Fanfair, C. Regens, G. L. Beutner, M. Lawler, P. Lobben, M. C. Soumeillant, B. Cohen, K. Zhu, D. Skliar, T. Rosner, C. E. Markwalter, Y. Hsiao, K. Tran and M. D. Eastgate, *J. Org. Chem.*, 2019, **84**, 4661–4669.
6 J. I. Murray, L. Zhang, A. Simon, M. V. S. Elipe, C. S. Wei, S. Caille and A. T. Parsons, *Org. Process Res. Dev.*, 2023, **27**, 198–205.
7 (*a*) S. E. Denmark, R. C. Smith and S. A. Tymonko, *Tetrahedron*, 2007, **63**, 5730–5738; (*b*) A. K. King, A. Brar and M. Findlater, *Catal. Sci. Technol.*, 2023, **13**, 301–304.
8 A. Côté, (*R,R*)-Me-DuPHOS Monoxide. *e-EROS Encycl.* Reagents, *Org. Synth.*, 2010, DOI: 10.1002/047084289X.rn01242.
9 S. Kotani, Y. Yoshiwara, M. Ogasawara, M. Sugiura and M. Nakajima, *Angew. Chem., Int. Ed.*, 2018, **57**, 15877–15881.
10 E. Mao, C. K. Chung, Y. Ji, Y.-h. Lam and P. E. Maligres, *J. Org. Chem.*, 2021, **86**, 7529–7536.
11 (*a*) S. E. García-Garrido, A. P. Soto and J. García-Álvarez, *Adv. Organomet. Chem.*, 2022, **77**, 105–168; (*b*) J. García-Álvarez, S. E. García-Garrido and V. Cadierno, *J. Organomet. Chem.*, 2014, **751**, 792–808; (*c*) A. Jain, H. Karmakar, P. W. Roesky and T. K. Panda, *Chem. Rev.*, 2023, **123**, 13323–13373.
12 A. Arques, D. Auñon and P. Molina, *Tetrahedron Lett.*, 2004, **45**, 4337–4340.
13 R. Venkateswaran, M. S. Balakrishna and S. M. Mobin, *Eur. J. Inorg. Chem.*, 2007, 1930–1938.

14 (*a*) Z.-X. Wang and L. Wang, *Chem. Commun.*, 2007, 2423–2425; (*b*) C. Zhang and Z.-X. Wang, *Organometallics*, 2009, **28**, 6507–6514.

15 (*a*) D. J. Law and R. G. Cavell, *J. Mol. Catal.*, 1994, **91**, 175–186; (*b*) T. T. Co, S. C. Shim, C. S. Cho, T. J. Kim, S. O. Kang, W.-S. Han, J. Ko and C.-K. Kim, *Organometallics*, 2005, **24**, 4824–4831; (*c*) S. Al-Benna, M. J. Sarsield, M. Thornton-Pett, D. L. Ormsby, P. J. Maddox, P. Bres and M. Bochmann, *J. Chem. Soc., Dalton Trans.*, 2000, 4247–4257.

16 (*a*) A. Buchard, H. Heuclin, A. Auffrant, X. F. Le Goff and P. Le Floch, *Dalton Trans.*, 2009, 1659–1667; (*b*) A. Buchard, E. Payet, A. Auffrant, X. Le Goff and P. Le Floch, *New J. Chem.*, 2010, **34**, 2943–2949.

17 V. D. M. Hoang, P. A. N. Reddy and T.-J. Kim, *Tetrahedron Lett.*, 2007, **48**, 8014–8017.

18 (*a*) L. Beaufort, F. Benvenuti, L. Delaude and A. F. Noels, *J. Mol. Catal. A: Chem.*, 2008, **283**, 77–82; (*b*) O. Alhomaidan, G. Bai and D. W. Stephan, *Organometallics*, 2008, **27**, 6343–6352; (*c*) D. Bézier, O. Daugulis and M. Brookhart, *Organometallics*, 2017, **36**, 2947–2951; (*d*) E. Martinez-Arripe, F. Jean-Baptiste-dit-Dominique, A. Auffrant, X.-F. Le Goff, J. Thuilliez and F. Nief, *Organometallics*, 2012, **31**, 4854–4861; (*e*) Z. Jian, A. R. Petrov, N. K. Hangaly, S. Li, W. Rong, Z. Mou, K. A. Rufanov, K. Harms, J. Sundermeyer and D. Cui, *Organometallics*, 2012, **31**, 4267–4282; (*f*) T. Cheisson, T.-P.-A. Cao, X. F. Le Goff and A. Auffrant, *Organometallics*, 2014, **33**, 6193–6399.

19 (*a*) E. M. Broderick, N. Guo, C. S. Vogel, C. Xu, J. Sutter, J. T. Miller, K. Meyer, P. Mehrhodavandi and P. Diaconescu, *J. Am. Chem. Soc.*, 2011, **133**, 9278–9281; (*b*) T.-P. Cao, A. Buchard, X. F. Le Goff, A. Auffrant and C. K. Williams, *Inorg. Chem.*, 2012, **51**, 2157–2169; (*c*) N. Yuntawattana, T. M. McGuire, C. B. Durr, A. Buchard and C. K. Williams, *Catal. Sci. Technol.*, 2020, **10**, 7226–7239; (*d*) M. T. Gamer, P. W. Roesky, I. Palard, M. Le Hellaye and S. M. Guillaume, *Organometallics*, 2007, **26**, 651–657; (*e*) Z. Mou, B. Liu, X. Liu, H. Xie, W. Rong, L. Li, S. Li and D. Cui, *Macromolecules*, 2014, **47**, 2233–2241; (*f*) H. Xie, Z. Mou, B. Liu, P. Li, W. Rong, S. Li and D. Cui, *Organometallics*, 2014, **33**, 722–730.

20 (*a*) M. G. Núñez, A. J. M. Farley and D. J. Dixon, *J. Am. Chem. Soc.*, 2013, **135**, 16348–16351; (*b*) M. Formica, D. Rozsar, G. Su, A. J. M. Farley and D. J. Dixon, *Acc. Chem. Res.*, 2020, **53**, 2235–2247; (*c*) X. Gao, J. Han and L. Wang, *Org. Lett.*, 2015, **17**, 4596–4599; (*d*) N. A. Richard, G. D. Charlton and C. A. Dyker, *Org. Biomol. Chem.*, 2021, **19**, 9167–9171; (*e*) M. Formica, T. Rogova, H. Shi, N. Sahara, B. Ferko, A. J. M. Farley, K. E. Christensen, F. Duarte, K. Yamazaki and D. J. Dixon, *Nat. Chem.*, 2023, **15**, 714–721; (*f*) S. Kotani, K. Yoshiwara, M. Ogasawara, M. Sugiura and M. Nakajima, *Angew. Chem., Int. Ed.*, 2018, **26**, 15877–15881.

21 S. S. Hanson, E. Doni, K. T. Traboulsee, G. Coulthard, J. A. Murphy and A. Dyker, *Angew. Chem., Int. Ed.*, 2015, **54**, 11236–11239.

22 (*a*) C. Bdenarek, I. Wehl, N. Jung, U. Schepers and S. Bräse, *Chem. Rev.*, 2020, **120**, 4301–4354; (*b*) Y. G. Gololobov and L. F. Kasukhin, *Tetrahedron*, 1992, **48**, 1353–1406.

23 A. V. Kirsanov, *Izv. Akad. Nauk SSSR, Ser. Khim.*, 1954, 646–655.

24 (*a*) L. Horner and H. Oediger, *Liebigs Ann.*, 1959, **627**, 142–162; (*b*) A. V. Kirsanov, *Izv. Akad. Nauk SSSR*, 1950, 426–437.

25 S. Bittner, M. Pomerantz, Y. Assaf, P. Krief, S. Xi and M. K. Witczak, *J. Org. Chem.*, 1988, **53**, 1–5.

26 *Bretherick's Handbook of Reactive Chemical Hazards*, ed. P. G. Urban, Butterworth-Heinemann, Ltd, Oxford, 6th edn, 1999. DOI: 10.1016/C2009-0-24106-7.

27 (*a*) H. Morita, A. Tatami, T. Maeda, B. J. Kim, W. Kawashima, T. Yoshimura and H. A. T. Akasaka, *J. Org. Chem.*, 2008, **73**, 7159–7163; (*b*) J.-J. Tang, X. Yu, Y. Wang, Y. Yamamoto and M. Bao, *Angew. Chem., Int. Ed.*, 2021, **60**, 16426–16435.

28 S. Lin, B. Lin, Z. Zhang, J. Chen, Y. Luo and Y. Xia, *Org. Lett.*, 2022, **24**, 3302–3306.

29 E. Falk, A. Franchino, T. Horak, L. Gürtler and B. Morandi, *Org. Lett.*, 2023, **25**, 1695–1700.

30 (*a*) N. E. S. Tay, D. Lehnherr and T. Rovis, *Chem. Rev.*, 2022, **122**, 2487–2649; (*b*) M. Yan, Y. Kawamata and P. S. Baran, *Chem. Rev.*, 2017, **117**, 13230–13319; (*c*) A. Wiebe, T. Gieshoff, S. Mohle, E. Rodrigo, M. Zirbes and S. R. Waldvogel, *Angew. Chem., Int. Ed.*, 2018, **57**, 5594–5619; (*d*) B. Cohen, D. Lehnherr, M. Sezen-Edmonds, J. H. Forstater, M. O. Fredrick, L. Deng, A. C. Ferretti, K. Harper and M. Diwan, *Chem. Eng. Res. Des.*, 2023, **192**, 622–637; (*e*) D. Lehnherr and L. Chen, *Org. Process Res. Dev.*, 2024, **28**, 338–366.

31 (*a*) E. C. Hansen, C. Li, S. Yang, D. Pedro and D. J. Weix, *J. Org. Chem.*, 2017, **82**, 7085–7092; (*b*) S. Kim, M. J. Goldfogel, M. M. Gilbert and D. J. Weix, *J. Am. Chem. Soc.*, 2020, **142**, 9902–9907; (*c*) A. L. Aguirre, N. L. Loud, K. A. Johnson, D. J. Weix and Y. Wang, *Chem.–Eur. J.*, 2021, **27**, 12981–129886.

32 (*a*) J. Rein, J. R. Annand, M. K. Wismer, J. Fu, J. C. Siu, A. Klapars, N. A. Strotman, D. Kalyani, D. Lehnherr and S. Lin, *ACS Cent. Sci.*, 2021, **7**, 1347–1355; (*b*) J. Rein, S. Lin, D. Kalyani and D. Lehnherr, High-Throughput Experimentation for Electrochemistry, in *The Power of High-Throughput Experimentation*, ed. D. C. Leitch, M. Jouffroy and M. Emmert, ACS Symposium Series, American Chemical Society, 2023, vol. 1419, pp. 167–187, DOI: 10.1021/bk-2022-1419.ch010.

33 HT*e*−Chem Electrochemistry, Analytical Sales and Services, Inc., https://www.analytical-sales.com/product-category/photoredox-parallel-synthesis/hte-chem-electrochemistry/, accessed April 15, 2023.

34 Both NMP and the tetraalkylammonium acetate supporting electrolyte are hygroscopic and were used as is without further drying prior to their use.

35 (*a*) F. Cozzi, *Adv. Synth. Catal.*, 2006, **348**, 1367–1390; (*b*) S. Itsuno and N. Haraguchi, Chapter 2: Catalysts Immobilized onto Polymers, in *Catalyst Immobilization: Methods and Applications*, ed. M. Benaglia and A. Puglis, Wiley, 2019, DOI: 10.1002/9783527817290.ch2.

36 T. Tannoux and A. Auffrant, *Coord. Chem. Rev.*, 2023, **474**, 214845.
37 (*a*) *Privileged Chiral Ligands and Catalysts*, ed. Q.-L. Zhou, Wiley, 2011, DOI: 10.1002/9783527635207; (*b*) T. P. Yoon and E. N. Jacobsen, *Science*, 2003, **299**, 1691–1693.
38 F. Richard, P. Clark, A. Hannam, T. Keenan, A. Jean and S. Arseniyadis, *Chem. Soc. Rev.*, 2024, **53**, 1936–1983.
39 We note that "triphos" has been used to described both "1,1,1-tris(diphenylphosphinomethyl)ethane" and "bis(diphenylphosphinoethyl)phenylphosphine" in the literature.
40 (*a*) G. Huttner, J. Strittmatter and S. Sandhoefner, Phosphorus Tripodal Ligands, in *Compr. Coord. Chem. II*, 2003, vol. 1, pp. 297–322, DOI: 10.1016/B0-08-043748-6/01082-3; (*b*) T. A. Betley and J. C. Peters, *J. Am. Chem. Soc.*, 2003, **125**, 10782–10783.
41 T. Güthner and B. Mertschenk, Cyanamides, in *Ullmann's Encyclopedia of Industrial Chemistry*, Wiley-VCH, Weinheim, 2006, DOI: 10.1002/14356007.a08_139.pub2.
42 NBO analysis predicted the spin density is localized at the phosphorus preferentially over being delocalized into the arene (see ESI† Table S14).
43 For an example of a domino electrolysis reaction, see previous reports on converting aldoximes to nitriles *via* oxidation to a nitrile oxide intermediate and subsequent reduction:(*a*) T. Shono, Y. Matsumura, K. Tsubata, T. Kamada and K. Kishi, *J. Org. Chem.*, 1989, **54**, 2249–2251; (*b*) M. F. Hartmer and S. R. Waldvogel, *Chem. Commun.*, 2015, **51**, 16346–16348.
44 For a 2nd example of a domino electrochemical reaction, see: X. Dong, J. L. Roeckl, S. R. Waldvogel and B. Morandi, *Science*, 2021, **371**, 507–514.
45 T. Wu and K. D. Moeller, Paired Electrolysis, in *Science of Synthesis: Electrochemistry in Organic Synthesis*, 2021, vol. 1, p. 481, DOI: 10.1055/sos-SD-236-00331.
46 C. A. Tolman, *Chem. Rev.*, 1977, **77**, 313–348.
47 D. G. Gusev, *Organometallics*, 2009, **28**, 763–770.
48 We note that limitations are known regarding the interpretation of TEP values, see: D. Cremer and E. Kraka, *Dalton Trans.*, 2017, **46**, 8323–8338.
49 Deposition numbers CCDC 2259467 (for **4**), 2259466 (for (*R*)-**25**), 2258974 (for **13**), 2258975 (for **24**), 2258976 (for **28**), 2258977 (for (*S*)-**33**), 2258978 (for **38**), 2258979 (for **39**), 2258980 (for **29**), and 2329725 (for **Ni-1**), contain the supplementary crystallographic data for this paper.
50 L. R. Favello, S. Fernández, M. M. García, R. Navarro and E. P. Urriolabeitia, *J. Chem. Soc., Dalton Trans.*, 1998, 3745–3750.
51 (*a*) S. Al-Benna, M. J. Sarsfield, M. Thornton-Pett, D. L. Ormsby, P. J. Maddox, P. Brès and M. Bochmann, *J. Chem. Soc., Dalton Trans.*, 2000, 4247–4257; (*b*) T. Cheisson, T.-P.-A. Cao, X. F. Le Goff and A. Auffrant, *Organometallics*, 2014, **33**, 6193–6199.
52 (*a*) D. J. Weix, *Acc. Chem. Res.*, 2015, **48**, 1767–1775; (*b*) M. C. Franke, V. R. Longley, M. Rafiee, S. S. Stahl, E. C. Hansen and D. J. Weix, *ACS Catal.*, 2022, **12**, 12617–12626; (*c*) S. Kim, M. J. Goldfogel, M. M. Gilbert and D. J. Weix, *J. Am. Chem. Soc.*, 2020, **142**, 9902–9907; (*d*) P. E. Piszel, B. Orzolek, A. K. Olszewski, M. Rotella, A. M. Spiewak, M. Kozlowski and D. J. Weix, *J. Am. Chem. Soc.*, 2023, **145**, 8517–8528.
53 (*a*) R. J. Perkins, D. J. Pedro and E. C. Hansen, *Org. Lett.*, 2017, **19**, 3755–3758; (*b*) R. J. Perkins, A. J. Hughes, D. J. Weix and E. C. Hansen, *Org. Process Res. Dev.*, 2019, **23**, 1746–1751.
54 (*a*) T. B. Hamby, M. J. LaLama and C. S. Sevov, *Science*, 2022, **376**, 410–416; (*b*) J. L. S. Zackasee, S. Al Zubaydi, B. L. Truesdell and C. S. Sevov, *ACS Catal.*, 2022, **12**, 1161–1166; (*c*) B. L. Truesdell, T. B. Hamby and C. S. Sevov, *J. Am. Chem. Soc.*, 2020, **142**, 5884–5893.
55 T. J. DeLano and S. E. Reisman, *ACS Catal.*, 2019, **9**, 6751–6754.
56 (*a*) C. E. I. Knappke, S. Grupe, D. Gärtner, M. Corpet, C. Gosmini and A. J. von Wangelin, *Chem.–Eur. J.*, 2014, 6828–6842; (*b*) D. J. Charboneau, H. Huang, E. L. Barth, C. C. Germe, N. Hazari, B. Q. Mercado, M. R. Uehling and S. L. Zultanski, *J. Am. Chem. Soc.*, 2021, **143**(49), 21024–21036; (*c*) H. A. Sakai, W. Liu, C. C. Le and D. W. C. MacMillan, *J. Am. Chem. Soc.*, 2020, **142**, 11691–11697; (*d*) F. Chen, K. Chen, Y. Zhang, Y. He, Y.-M. Wang and S. Zhu, *J. Am. Chem. Soc.*, 2017, **139**, 13929–13935; (*e*) J. Zhou, D. Wang, W. Xu, Z. Hu and T. Xu, *J. Am. Chem. Soc.*, 2023, **145**, 2081–2087; (*f*) W. Zhang, L. Lu, W. Zhang, Y. Wang, S. D. Ware, J. Mondragon, J. Rein, N. Strotman, D. Lehnherr, K. A. See and S. Lin, *Nature*, 2022, **604**, 292–297; (*g*) J. Liao, C. H. Basch, M. E. Hoerrner, M. R. Talley, B. P. Boscoe, J. W. Tucker, M. R. Garnse and M. P. Watson, *Org. Lett.*, 2019, **21**, 2941–2946; (*h*) J. Twilton, M. R. Johnson, V. Sidana, M. C. Franke, C. Bottecchia, D. Lehnherr, F. Lévesque, S. M. M. Knapp, L. Wang, J. B. Gerken, C. M. Hong, T. P. Vickery, M. D. Weisel, N. A. Strotman, D. J. Weix, T. W. Root and S. S. Stahl, *Nature*, 2023, **623**, 71–76.
57 (*a*) A. Conan, S. Sibille, E. d'Incan and J. Périchon, *J. Chem. Soc. Chem. Commun.*, 1990, 48–49; (*b*) M. Durandetti, J.-Y. Nédélec and J. Périchon, *J. Org. Chem.*, 1996, **61**, 1748–1755; (*c*) M. Durandetti, J. Périchon and J.-Y. Nédélec, *J. Org. Chem.*, 1997, **62**, 7914–7915.
58 C. S. Day, A. Rentería-Gómez, S. J. Ton, A. R. Gogoi, O. Gutierrez and R. Martin, *Nat. Catal.*, 2023, **6**, 244–253.
59 T. Tang, A. Hazra, D. S. Min, W. L. Williams, E. Jones, A. G. Doyle and M. S. Sigman, *J. Am. Chem. Soc.*, 2023, **145**, 8689–8699.
60 (*a*) P. A. Cox, A. G. Leach, A. D. Campbell and G. C. Lloyd-Jones, *J. Am. Chem. Soc.*, 2016, **138**, 9145–9157; (*b*) P. A. Cox, M. Reid, A. G. Leach, A. D. Campbell, E. J. King and G. C. Lloyd-Jones, *J. Am. Chem. Soc.*, 2017, **139**, 13156–13165.
61 L. K. G. Ackerman, M. M. Lovell and D. J. Weix, *Nature*, 2015, **524**, 454–457.
62 I. B. Perry, T. F. Brewer, P. J. Sarver, D. M. Schultz, D. A. DiRocco and D. W. C. MacMillan, *Nature*, 2018, **560**, 70–75.

63 (*a*) V. T. Tran, N. Kim, C. Z. Rubel, X. Wu, T. Kang, T. C. Jankins, Z.-Q. Li, M. V. Joannou, S. Ayers, M. Gembicky, J. Bailey, E. J. Sturgell, B. B. Sanchez, J. S. Chen, S. Lin, M. D. Eastgate, S. R. Wisniewski and K. M. Engle, *Angew. Chem., Int. Ed.*, 2023, **62**, e202211794; (*b*) C. Z. Rubel, W.-J. He, S. R. Wisniewski and K. M. Engle, *Acc. Chem. Res.*, 2024, **57**, 312–326.

64 H. Hu, A. N. Singh, D. Lehnherr, V. Mdluli, S. W. Chun, A. M. Makarewicz, J. R. Gouker, O. Ukaegbu, S. Li, X. Wen, D. G. McLaren, J. E. Velasquez, J. C. Moore, S. Galanie, E. Appiah-Amponsah and E. L. Regalado, *Anal. Chem.*, 2024, **96**, 1138–1146.

65 (*a*) C. Li, Y. Kawamata, H. Nakamura, J. C. Vantourout, Z. Liu, Q. Hou, D. Bao, J. T. Starr, J. hen, M. Yan and P. S. Baran, *Angew. Chem., Int. Ed.*, 2017, **56**, 13088–13093; (*b*) Y. Kawamata, J. C. Vantourout, D. P. Hickey, P. Bai, L. Chen, Q. Hou, W. Qiao, K. Barman, M. A. Edwards, A. F. Garrido-Castro, J. N. deGruyter, H. Nakamura, K. Knouse, C. Qin, K. J. Clay, D. Bao, C. Li, J. T. Starr, C. Garcia-Irizarry, N. Sach, H. S. White, M. Neurock, S. D. Minteer and P. S. Baran, *J. Am. Chem. Soc.*, 2019, **141**, 6392–6402; (*c*) S. Sengmany, F. Daili, I. Kribii and E. Léonel, *J. Org. Chem.*, 2023, **88**, 675–683.

66 After a pre-print of this work was posted online, a different electrochemical approach to *N*-aryl iminophosphoranes was reported, see: (*a*) V. Mdluli, D. Lehnherr, Y.-h. Lam, M. T. Chaudhry, J. A. Newman, J. O. DaSilva and E. L. Regalado, *ChemRxiv*, 2023, preprint, DOI: **10.26434/chemrxiv-2023-f7d2q**; (*b*) R. C. e. Silva, C. Vega, M. Regnier, L. Capaldo, L. Wesenberg, G. Lowe, K. T. de Oliveira and T. Noël, *Adv. Synth. Catal.*, 2024, **366**, 955–960.

67 S. Kashimura and K. Matsumoto, Electrogenerated Base, in *Encyclopedia of Applied Electrochemistry*, ed. G. Kreysa, K. Ota and R. F. Savinell, Springer, 2014, New York, NY, DOI: **10.1007/978-1-4419-6996-5_354**.

68 (*a*) F. D. Marsh and E. Hermes, *J. Am. Chem. Soc.*, 1964, **86**, 4506–4507; (*b*) D. Goldsmith, Cyanogen azide, in *Encyclopedia of Reagents for Organic Synthesis*, E-EROS Encyclopedia of Reagents for Organic Synthesis, 2001, DOI: **10.1002/047084289X.rc268**, 978-0471936237; (*c*) F. D. Marsh, *J. Org. Chem.*, 1972, **37**, 2966–2969; (*d*) R. Matyáš, J. Pachman, *Primary Explosives*, Springer Science & Business Media, 12 March 2013, p. 111; (*e*) M. L. Madigan, *First Responders Handbook: An Introduction*, CRC Press, Second Edition, 13 September 2017, p. 170.